

# Spontaneous Formation of Magnetic Flux Concentrations in Stratified Turbulence

Koen Kemel · Axel Brandenburg · Nathan Kleeorin ·  
Dhrubaditya Mitra · Igor Rogachevskii

Received: 2 December 2011 / Accepted: 13 February 2012 / Published online: 20 March 2012  
© Springer Science+Business Media B.V. 2012

**Abstract** The negative effective magnetic pressure instability discovered recently in direct numerical simulations (DNSs) may play a crucial role in the formation of sunspots and active regions in the Sun and stars. This instability is caused by a negative contribution of turbulence to the effective mean Lorentz force (the sum of turbulent and non-turbulent contributions) and results in the formation of large-scale inhomogeneous magnetic structures from an initially uniform magnetic field. Earlier investigations of this instability in DNSs of stably stratified, externally forced, isothermal hydromagnetic turbulence in the regime of large plasma  $\beta$  are now extended into the regime of larger scale separation ratios where the number of turbulent eddies in the computational domain is about 30. Strong spontaneous formation of large-scale magnetic structures is seen even without performing any spatial averaging. These structures encompass many turbulent eddies. The characteristic time of the instability is comparable to the turbulent diffusion time,  $L^2/\eta_t$ , where  $\eta_t$  is the turbulent diffusivity and  $L$  is the scale of the domain. DNSs are used to confirm that the effective magnetic pressure does indeed become negative for magnetic field strengths below the equipartition field. The dependence of the effective magnetic pressure on the field strength is characterized by fit parameters that seem to show convergence for larger values of the magnetic Reynolds number.

**Keywords** Magnetohydrodynamics (MHD) · Sun: dynamo · Sunspots · Turbulence

---

Advances in European Solar Physics

Guest Editors: Valery M. Nakariakov, Manolis K. Georgoulis, and Stefaan Poedts

K. Kemel · A. Brandenburg (✉) · N. Kleeorin · D. Mitra · I. Rogachevskii  
Nordita, AlbaNova University Center, Roslagstullsbacken 23, 10691 Stockholm, Sweden  
e-mail: [brandenb@nordita.org](mailto:brandenb@nordita.org)

K. Kemel · A. Brandenburg  
Department of Astronomy, Stockholm University, 10691 Stockholm, Sweden

N. Kleeorin · I. Rogachevskii  
Department of Mechanical Engineering, Ben-Gurion University of the Negev, POB 653,  
Beer-Sheva 84105, Israel

## 1. Introduction

The 11-year solar activity cycle manifests itself through a periodic variation of the sunspot number. Sunspots consist of vertical magnetic fields with a strength of up to 3 kG in their center (see, e.g., Parker, 1979; Ossendrijver, 2003). It is generally believed that these fields also continue in a similarly concentrated fashion beneath the surface in the form of magnetic flux tubes or fibers (Parker, 1982). It was thought that fibral magnetic fields constitute a lower energy state and might therefore be preferred (Parker, 1984). Tube-like magnetic fields were frequently seen in hydromagnetic turbulence simulations (Nordlund *et al.*, 1992; Brandenburg, Procaccia, and Segel, 1995; Brandenburg *et al.*, 1996), yet those tubes were similar to the vortex tubes in hydrodynamic turbulence. Such vortex tubes have typical diameters comparable to the viscous length; similarly, the aforementioned magnetic tubes seen in simulations have a thickness comparable to the resistive length. However, for the Sun, the resulting tube thickness would be too small to be relevant for sunspots.

At the surface, strong magnetic flux concentrations also form in regions of strong flow convergence, but the size of these regions is too small for sunspots, because sunspots are usually much bigger than a single granular convection cell. In fact, a typical sunspot can have a diameter of some 30 pressure scale heights. The tremendous size of sunspots has therefore been used as an argument that they do not form near the surface, but at much greater depths near the bottom of the convection zone. At the bottom of the convection zone the convection cells are big enough and could in principle be responsible for producing much bigger flux concentrations. Magnetic flux tubes can also form through the action of shear, as shown by various simulations (Cline, Brummell, and Cattaneo, 2003; Guerrero and Käpylä, 2011). However, again it is possible that the size of such flux structures is related to the resistive scale and therefore too small. While shear is likely an important ingredient of the solar dynamo, it remains unclear whether the resulting magnetic tubes are really able to produce sunspots as a result of their piercing through the solar surface and, more importantly, whether one should consider them as being tied to the deep shear layers of the Sun.

In this paper we discuss an alternative scenario in which sunspots are shallow phenomena that are not anchored at the bottom of the convection zone. Various mechanisms have been discussed, but of particular interest here are mechanisms that are based on the suppression of turbulence by magnetic fields. In the mechanism of Kitchatinov and Mazur (2000) it is the suppression of the turbulent heat flux, while in the mechanism of Rogachevskii and Kleerorin (2007) it is the suppression of the turbulent hydromagnetic pressure. Both mechanisms lead to a linear large-scale instability in a stratified medium. However, these mechanisms may be of different importance in different layers.

In this study we focus mainly on the second mechanism, which has recently been studied in direct numerical simulations (DNSs) as well as in mean-field calculations. This mechanism is called the negative effective magnetic pressure instability (NEMPI). It is a convective type instability that is similar to the interchange instability in plasmas (Tserkovnikov, 1960; Newcomb, 1961; Priest, 1982) and the magnetic buoyancy instability (Parker, 1966). However, the free energy in interchange and magnetic buoyancy instabilities is due to the gravitational field, while in NEMPI it is provided by the small-scale turbulence. NEMPI is caused by the suppression of turbulent hydromagnetic pressure by the mean magnetic field. When the hydrodynamic Reynolds number is larger than unity and the mean magnetic field is less than the equipartition field strength, the negative turbulent contribution to the mean Lorentz force is large enough so that the effective mean magnetic pressure (the sum of turbulent and non-turbulent contributions) becomes negative (Kleerorin, Rogachevskii, and Ruzmaikin, 1989, 1990; Rogachevskii and Kleerorin, 2007). This is the main reason for the

excitation of the large-scale instability that results in the formation of large-scale inhomogeneous magnetic structures.

The effect of the suppression of the turbulent heat flux has not yet been studied as extensively as NEMPI. An exception is the work of Kitchatinov and Olemskoy (2006), who have used the model of Kitchatinov and Mazur (2000) to study the decay of sunspots. Moreover, there is now some evidence that the effects anticipated by Kitchatinov and Mazur (2000) may have already been in operation in various simulations of solar convection where the spontaneous formation of pores has been seen (Stein *et al.*, 2011). Such pores are of the size of several granules, but one may hope that the step toward structures of the size of active regions is a quantitative one that is controlled by the amount of flux present. Another example is the large-eddy simulation of Kitiashvili *et al.* (2010), where an imposed vertical large-scale magnetic field is concentrated into giant vortices. This result is reminiscent of that of Tao *et al.* (1998), who found a segregation into magnetized and nearly unmagnetized regions in stratified convection simulations. However, it has not yet been possible to obtain large-scale magnetic structures resembling sunspots, except in models with a strong imposed magnetic flux tube structure at the bottom of the domain (see, *e.g.*, Rempel, Schüssler, and Knölker, 2009; Rempel *et al.*, 2009; Cheung *et al.*, 2010; Rempel, 2011a, 2011b). Such simulations demonstrate quite clearly that many aspects of sunspot formation are now well understood. However, the physics involved in these simulations must become part of a larger picture in which the need for manually imposed flux concentrations is relaxed by self-consistently modeling their formation. Whether such flux concentrations originate from the tachocline (*e.g.*, Cally, Dikpati, and Gilman, 2003) or from the upper layers remains an open question (Brandenburg, 2005). Here we focus on the latter scenario, where both NEMPI and the suppression of convective heat flux have been discussed.

In the rest of this paper, we focus on NEMPI, which was first found in mean-field calculations of a stratified layer (Kleeorin, Mond, and Rogachevskii, 1996; Rogachevskii and Kleeorin, 2007; Brandenburg, Kleeorin, and Rogachevskii, 2010; Kemel *et al.*, 2012). However, those results remained unconvincing until NEMPI was also discovered in DNS (Brandenburg *et al.*, 2011, hereafter BKKMR). It is therefore most appropriate to begin our discussion with the latter.

## 2. The Model

Following the earlier work of BKKMR, we solve the equations for the velocity  $\mathbf{U}$ , the magnetic vector potential  $\mathbf{A}$ , and the density  $\rho$ ,

$$\rho \frac{D\mathbf{U}}{Dt} = -c_s^2 \nabla \rho + \mathbf{J} \times \mathbf{B} + \rho(\mathbf{f} + \mathbf{g}) + \nabla \cdot (2\nu\rho\mathbf{S}), \quad (1)$$

$$\frac{\partial \mathbf{A}}{\partial t} = \mathbf{U} \times \mathbf{B} + \eta \nabla^2 \mathbf{A}, \quad (2)$$

$$\frac{\partial \rho}{\partial t} = -\nabla \cdot \rho \mathbf{U}, \quad (3)$$

where  $\nu$  is the kinematic viscosity,  $\eta$  is the magnetic diffusivity due to Spitzer conductivity of the plasma,  $\mathbf{B} = \mathbf{B}_0 + \nabla \times \mathbf{A}$  is the magnetic field,  $\mathbf{B}_0 = (0, B_0, 0)$  is the imposed uniform field,  $\mathbf{J} = \nabla \times \mathbf{B}/\mu_0$  is the current density,  $\mu_0$  is the vacuum permeability, and  $\mathbf{S}_{ij} = \frac{1}{2}(\partial_i U_j + \partial_j U_i) - \frac{1}{3}\delta_{ij}\nabla \cdot \mathbf{U}$  is the traceless rate of strain tensor. The forcing function  $\mathbf{f}$  consists of random, white-in-time, non-polarized plane waves with a certain average

wavenumber  $k_f$ . The forcing strength is such that the turbulent rms velocity is approximately independent of  $z$  with  $u_{\text{rms}} = \langle \mathbf{u}^2 \rangle^{1/2} \approx 0.1 c_s$ . We consider a domain of size  $L_x \times L_y \times L_z$  in Cartesian coordinates  $(x, y, z)$ , with periodic boundary conditions in the  $x$  and  $y$  directions and stress-free perfectly conducting boundaries at top and bottom ( $z = \pm L_z/2$ ). The volume-averaged density is therefore constant in time and equal to its initial value,  $\rho_0 = \langle \rho \rangle$ . The gravitational acceleration  $\mathbf{g} = (0, 0, -g)$  is chosen such that  $k_1 H_\rho = 1$ , which leads to a density contrast between bottom and top of  $\exp(2\pi) \approx 535$ , where  $k_1 = 2\pi/L_z$  is the lowest wavenumber in the domain and  $H_\rho = c_s^2/g$  is the density scale height. Thus  $L_z/H_\rho = 2\pi$ , so the domain extends in the vertical direction over approximately six scale heights.

Our simulations are characterized by the scale separation ratio,  $k_f/k_1$ , the fluid Reynolds number  $\text{Re} \equiv u_{\text{rms}}/\nu k_f$ , the magnetic Prandtl number  $\text{Pr}_M = \nu/\eta$ , and the magnetic Reynolds number  $\text{Re}_M \equiv \text{Re} \text{Pr}_M$ . Following earlier work (Brandenburg *et al.*, 2012), it is clear that NEMPI is more effective for small values of  $\text{Pr}_M$ , so here we choose  $\text{Pr}_M = 0.5$  and  $\text{Re}_M$  in the range  $0.7 - 70$ . The magnetic field is expressed in units of the local equipartition field strength,  $B_{\text{eq}} = \sqrt{\mu_0 \rho_0 u_{\text{rms}}}$ , while  $B_0$  is specified in units of the volume-averaged value,  $B_{\text{eq}0} = \sqrt{\mu_0 \rho_0 u_{\text{rms}}}$ . Note that  $B_{\text{eq}}(z) = B_{\text{eq}0} \sqrt{\rho(z)/\rho_0}$ . In addition to visualizations of the actual magnetic field, we also monitor  $\Delta \bar{B}_y = \bar{B}_y - B_0$ , where  $\bar{B}_y$  is an average over  $y$  and a certain time interval  $\Delta t$ . Time is expressed in eddy turnover times,  $\tau_{\text{to}} = (u_{\text{rms}} k_f)^{-1}$ . This is the relevant adjustment time to the application of a magnetic field, for example. It is also the relevant time scale for small-scale dynamo action. For comparison, we also consider the turbulent-diffusive time scale,  $\tau_{\text{td}} = (\eta_{10} k_1^2)^{-1}$ , where  $\eta_{10} = u_{\text{rms}}/3k_f$  is the estimated turbulent magnetic diffusivity. This is the time scale relevant for mean-field phenomena such as those discussed here. Another diagnostic quantity is the rms magnetic field in the Fourier mode of  $k = k_1$ , referred to as  $B_1$ , which is taken here as an average over  $2 \leq k_1 z \leq 3$ , and is close to the top at  $k_1 z = \pi$  (note that  $B_1$  does not include the imposed field  $B_0$  at  $k = 0$ ). We have chosen this  $z$  range because it is the one where the instability appears first; therefore, it is best seen in that range.

The simulations are performed with the PENCIL CODE,<sup>1</sup> which uses sixth-order explicit finite differences in space and a third-order accurate time stepping method. We use numerical resolutions of  $128^3$  and  $256^3$  mesh points when  $L_x = L_y = L_z$ , and  $1024 \times 128^2$  when  $L_x = 8L_y = 8L_z$ . To capture mean-field effects on the slower turbulent-diffusive time scale, which is  $\tau_{\text{td}}/\tau_{\text{to}} = 3k_f^2/k_1^2$  times slower than the dynamical time scale, we perform simulations for several thousand turnover times.

### 3. Results

In simulations, the clearest indication of a spontaneous flux concentration is seen when the scale separation ratio is large. In BKKMR, we only used  $k_f/k_1 = 15$ . Here we consider calculations where this ratio is twice as large. A useful diagnostic is the magnetic field averaged along the direction of the imposed field, *i.e.*, along the  $y$  direction. In particular, we shall be looking at the  $y$  component of the field, *i.e.*,  $\langle \Delta B_y \rangle_y / B_{\text{eq}}$ . To see the effect even more clearly, we perform an additional time average over about 100 turnover times. This average is then referred to as  $\langle \Delta B_y \rangle_{yt}$ . In Figure 1 we show  $\langle \Delta B_y \rangle_{yt} / B_{\text{eq}}$  for  $k_f/k_1 = 30$ . The other parameters are  $\text{Re}_M = 18$  and  $\text{Pr}_M = 0.5$ . An inhomogeneous magnetic structure forms first near the surface (at  $t/\tau_{\text{td}} = 0.79$ ), but then the structure propagates downward. This is

<sup>1</sup><http://pencil-code.googlecode.com>.

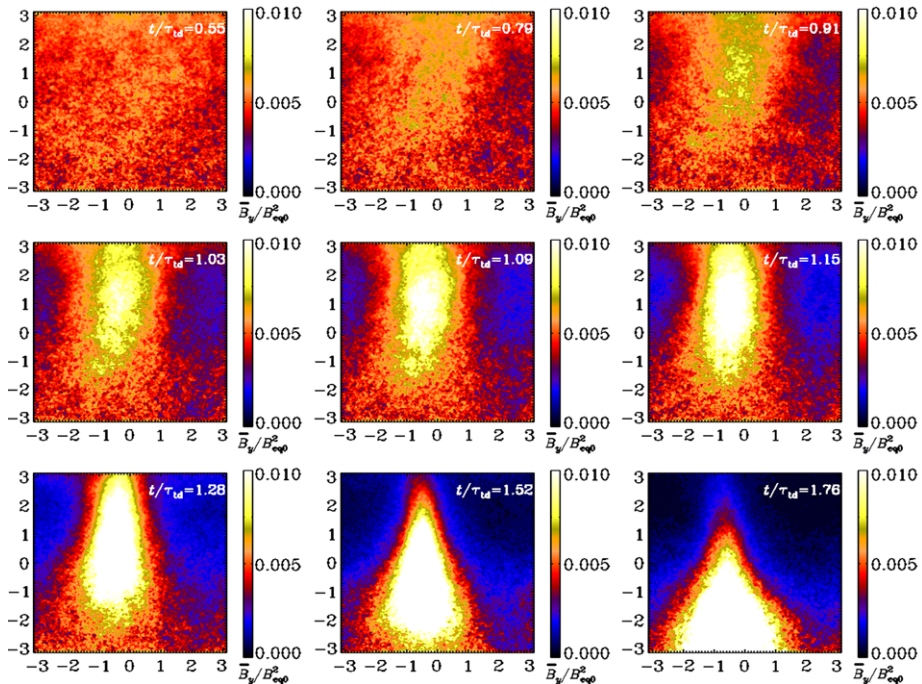


**Figure 1** Visualizations of  $\langle \Delta B_y \rangle_y(x, z, t)$  for different times. Time is indicated in turbulent-diffusive times,  $(\eta_{l0} k_1^2)^{-1}$ , corresponding to about 5000 turnover times, *i.e.*,  $t = 5000/u_{\text{rms}}k_f$ , and the dimensions in the horizontal and vertical directions are in units of  $H_\rho$ .  $\text{Re}_M = 18$  and  $\text{Pr}_M = 0.5$ .

consistent with our interpretation that this is caused by negative effective magnetic pressure operating on the scale of many turbulent eddies. Indeed, a local decrease of the effective magnetic pressure must be compensated by an increase in gas pressure, which implies higher density, so the structure becomes heavier and sinks in the nonlinear stage of NEMPI. This is also seen in three-dimensional visualizations without averaging; see Figure 2 with the same parameters as in Figure 1. The top view of this figure justifies our assumption that the structures are two dimensional, and that averaging over the  $y$  direction was therefore meaningful.

To confirm that NEMPI really is a large-scale instability, we would expect to see an exponential growth phase. This is shown in the right-hand panel of Figure 3, where we show the growth of  $B_1$  versus time. We recall that  $B_1$  measures the magnetic field variation near the top layer in  $2 \leq k_1 z \leq 3$ ; note that the equipartition field used for normalization is also averaged over this layer. We give time both in turbulent-diffusive times (lower abscissa) as well as in eddy turnover times (upper abscissa). We do see that there is an exponential growth phase which lasts for about one turbulent-diffusive time; *i.e.*, the growth rate is comparable to  $(\eta_{l0} k^2)^{-1}$ , where  $\eta_l \approx u_{\text{rms}}/3k_f$  is the expected turbulent magnetic diffusivity (Sur, Brandenburg, and Subramanian, 2008). However, compared with the eddy turnover time,  $(u_{\text{rms}}k_f)^{-1}$ , the turbulent-diffusive time scale is  $3(k_f/k_1)^2$  times slower. This illustrates that NEMPI is indeed a very slow process compared with, for example, the saturation of the overall rms magnetic field (left-hand panel of Figure 3).

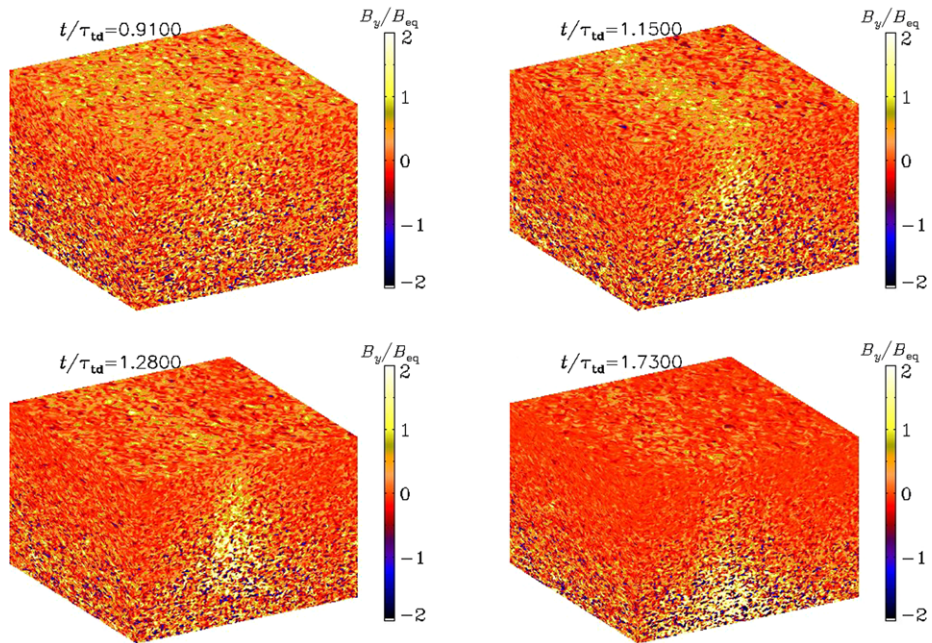


**Figure 2** Visualizations of  $B_y$  on the periphery of the domain for different times, indicated in turbulent–diffusive times, for the same run as in Figure 1.

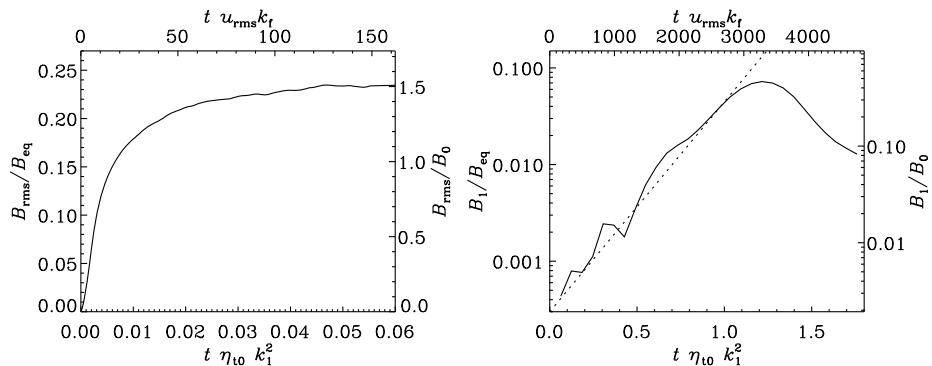


**Figure 3** Time dependence of  $B_{\text{rms}}$  (left panel) and  $B_1$  (right panel) for the same run as in Figure 1, where  $k_f/k_1 = 30$  and  $B_0/B_{\text{eq}} = 0.05$ .

Given that the magnetic field structures sink through this layer during the late nonlinear evolution, it is not surprising that  $B_1$  in Figure 3 drops after having reached a maximum at  $t\eta_{10}k_1^2 \approx 1$ .

While the rate of NEMPI may be too slow to explain the relatively rapid appearance of sunspots on a time scale of days, it would explain how one can produce magnetic structures on length and time scales much bigger than the naturally occurring scales in the upper layers of the Sun. This size discrepancy is exactly one of the reasons why one normally places the

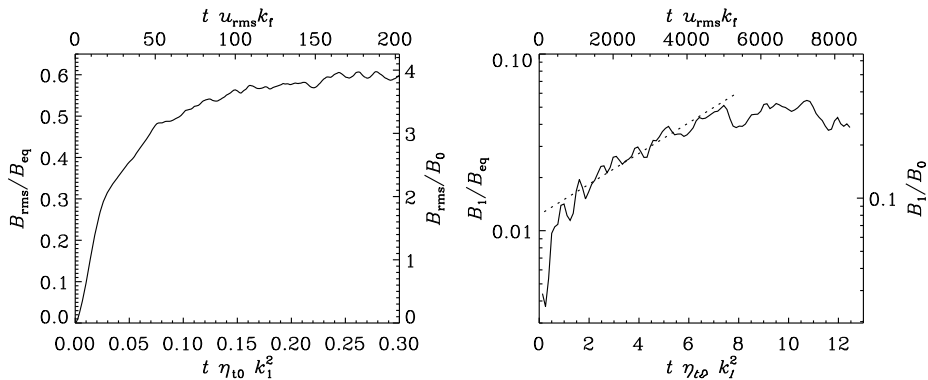


**Figure 4** Time dependence of  $B_{\text{rms}}$  (left panel) and  $B_1$  (right panel) for a run used in BKKMR with  $k_f/k_1 = 15$  and  $B_0/B_{\text{eq}0} = 0.05$ , but for a resolution of  $256^3$  mesh points.

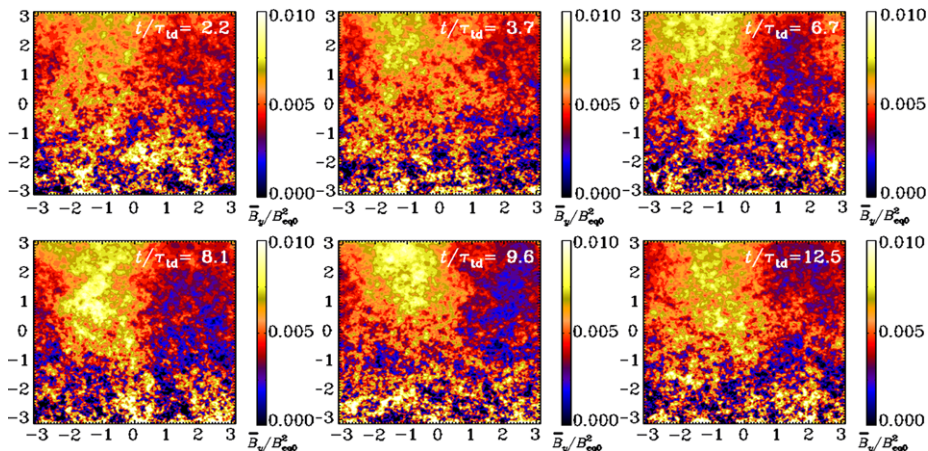


**Figure 5** Same as Figure 1, but for the run with  $k_f/k_1 = 15$ .  $\text{Re}_M = 36$  and  $\text{Pr}_M = 0.5$ .

formation of active regions at the bottom of the convection zone (Golub *et al.*, 1981). Here we see a clear example that this conclusion may not be correct.

Next, we turn to a simulation where the scale separation ratio,  $k_f/k_1$ , is only half as big, *i.e.*,  $k_f/k_1 = 15$ . In that case we also see an exponential growth phase, but the growth is slower (even in terms of turbulent-diffusive times), lasts longer, and amplifies  $B_1$  only by about one order of magnitude; see Figure 4. Although there is also a slight decline of  $B_1$  after the end of the exponential growth phase, this decline appears to be milder and the structures do not seem to sink to the same extent as in the case with  $k_f/k_1 = 30$ , as can be seen from visualizations of  $\langle \Delta B_y \rangle_{yt}$  in Figure 5. These structures are also poorly discernible in individual snapshots; see Figure 6.

Again, in agreement with related work involving the suppression of turbulent heat flux, the most unstable mode has a horizontal wavelength comparable to the vertical scale height of the layer; see Figure 2 of Kitchatinov and Mazur (2000). For NEMPI this is shown in Figure 7, where we compare an instantaneous plot of  $\langle \Delta B_y \rangle_y(x, z)$  with a time-averaged one,  $\langle \Delta B_y \rangle_{yt}$ , making the appearance of large-scale structures more pronounced. Next, in

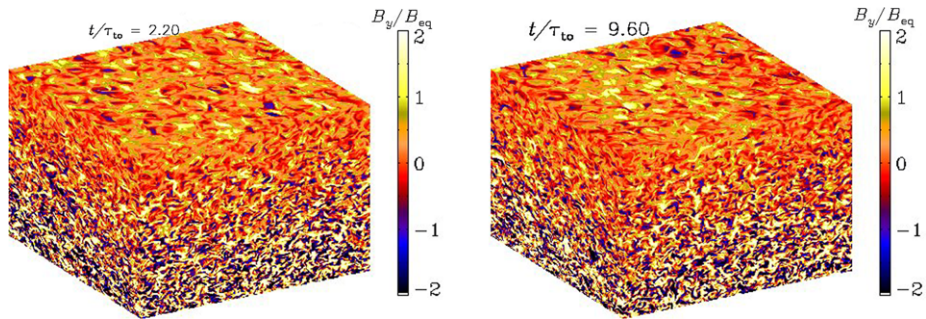


**Figure 6** Visualizations of  $B_y$  on the periphery of the domain for the run with  $k_f/k_1 = 15$  and two times that are also shown in Figure 5. Note some slight enhancement of the field in the left part of the domain at late times.

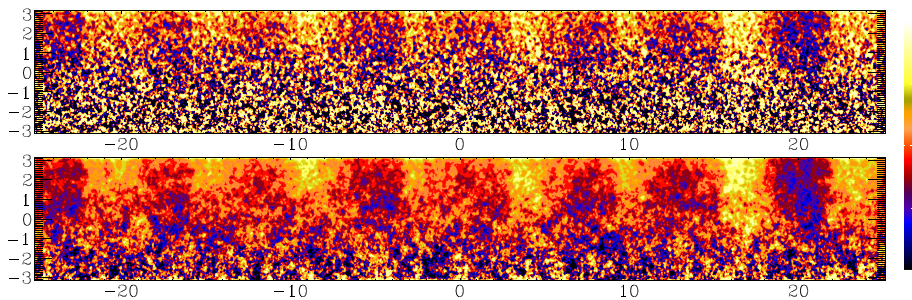


**Figure 7** Visualization of  $\overline{B}_y(x, z)$  for an elongated box ( $1024 \times 128^2$  mesh points) with  $Re_M = 36$  at a time during the statistically steady state. The top panel shows the  $y$  average  $\langle \Delta B_y \rangle_y / B_{eq}$  at one time while the lower panel shows an additional time average  $\langle \Delta B_y \rangle_{yt} / B_{eq}$  covering about 80 turnover times. The dimensions in the horizontal and vertical directions are  $H_\rho$ , so the extent is  $16\pi H_\rho \times 2\pi H_\rho$ .

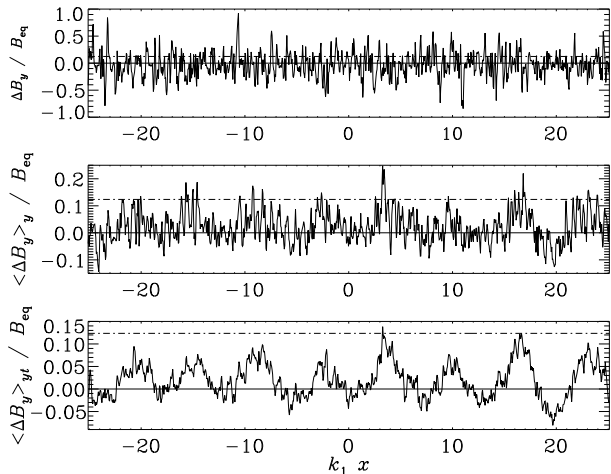
Figure 8 we compare cross sections of  $\Delta B_y(x)$  (for fixed values of  $y$ ,  $z$ , and  $t$ ; top panel) with corresponding  $y$  averages (middle panel) and  $yt$  averages (bottom panel). Here,  $Re_M = 36$ ,  $k_f/k_1 = 15$ , and  $B_0/B_{eq0} = 0.05$ . Without averaging, no clear magnetic structure is seen yet, but the structures become clearly more pronounced with  $y$  and  $t$  averaging. Runs with similar parameters have been shown in BKKMR for a computational domain whose  $x$  extent is  $2\pi/k_1$  instead of  $16\pi/k_1$ .

The large-scale flux concentrations have an amplitude of only  $B_1 \approx 0.1 B_{eq}$  and are therefore not easily seen in single snapshots, where the field reaches peak strengths comparable to  $B_{eq}$ . Furthermore, as for any linear instability, the flux concentrations form a repetitive pattern, and are in that sense similar to flux concentrations seen in the calculations of Kitchatinov and Mazur (2000) that were based on the magnetic suppression of the turbulent heat flux. However, there are indications that, at larger values of  $Re_M$ , flux concentrations occur more rarely, which might be more realistic in view of astrophysical applications.

#### 4. Quantifying the Negative Effective Magnetic Pressure Effect

An important condition for the formation of structures by the mechanisms of Kitchatinov and Mazur (2000) and Rogachevskii and Kleeorin (2007) is sufficient scale separation. In

**Figure 8**  $x$  dependence of the field for an elongated box ( $1024 \times 128^2$  mesh points) with  $\text{Re}_M = 36$  at  $k_1 z = 2$  (*i.e.*, near the top of the domain) showing  $\Delta B_y / B_{\text{eq}}$  at  $y = 0$  (top panel), its  $y$  average  $\langle \Delta B_y \rangle_y / B_{\text{eq}}$  (middle panel), as well as an additional time average  $\langle \Delta B_y \rangle_{yt} / B_{\text{eq}}$  (bottom panel) covering about 80 turnover times. The dash-dotted line gives the level of the imposed field.



other words, both the suppression of convective heat flux and the suppression of total effective pressure have in common that they only work if a substantial number of eddies is involved in a turbulent structure under consideration. If this is not the case, turbulent transport coefficients become increasingly inefficient. This is a natural feature of large-scale effects such as this one. Here, we mean by turbulent transport coefficients any of the mean-field coefficients that relate correlation functions of small-scale quantities to expressions given in terms of large-scale quantities.

Small- and large-scale quantities refer here simply to a suitably defined averaging procedure so that the velocity  $\mathbf{U}$ , for example, can be split into a mean (or large-scale) quantity  $\overline{\mathbf{U}}$  and a fluctuation  $\mathbf{u} = \mathbf{U} - \overline{\mathbf{U}}$ . An important example of a turbulent transport coefficient is the turbulent viscosity that emerges when relating the Reynolds stress  $\overline{u_i u_j}$  to the spatial derivatives of the mean flow  $\overline{\mathbf{U}}$  in the averaged momentum equation,

$$\frac{\partial}{\partial t} \overline{\rho} \overline{U}_i = - \frac{\partial}{\partial x_j} (\overline{\rho} \overline{U}_i \overline{U}_j + \overline{\rho} \overline{u}_i \overline{u}_j + \dots). \quad (4)$$

Here,  $\overline{\rho}$  is the average density, and correlations with density fluctuations are neglected. The simplest parameterization for  $\overline{u_i u_j}$  is

$$\overline{u_i u_j} = -\nu_t (\overline{U}_{i,j} + \overline{U}_{j,i}) - \mu_t \delta_{ij} \nabla \cdot \overline{\mathbf{U}}, \quad (5)$$

where  $\nu_t$  is the turbulent shear viscosity and  $\mu_t$  is the turbulent bulk viscosity. This relation is also known as the Boussinesq ansatz, especially when contrasted with representations where the  $\Lambda$  effect is included, which is responsible for producing differential rotation in the Sun (Rüdiger, 1989). However, here we shall focus on magnetic effects.

In general, when there are magnetic fields, the right-hand side of equation of motion (4) must be replaced by the sum of Reynolds and Maxwell stresses

$$\overline{\Pi}_{ij}^f \equiv \overline{\rho} \overline{u_i u_j} - \overline{b_i b_j} / \mu_0 + \frac{1}{2} \overline{\mathbf{b}^2} / \mu_0, \quad (6)$$

where the superscript  $f$  indicates contributions from the fluctuating field. In the absence of a mean magnetic field, this stress,  $\overline{\Pi}_{ij}^{f,0}$ , has finite contributions from  $\nu_t$ ,  $\mu_t$ , the  $\Lambda$  effect, and perhaps other terms. We are now interested in the excess,

$$\Delta \overline{\Pi}_{ij}^f = \overline{\Pi}_{ij}^{f,\overline{\mathbf{B}}} - \overline{\Pi}_{ij}^{f,0}, \quad (7)$$

that is caused solely by the presence of  $\bar{\mathbf{B}}$ . The only tensors that can be constructed with  $\bar{\mathbf{B}}$  are those proportional to  $\delta_{ij}\bar{\mathbf{B}}^2$  and  $\bar{B}_i\bar{B}_j$ . This leads to the ansatz

$$\Delta\bar{\Pi}_{ij}^f = q_s\bar{B}_i\bar{B}_j/\mu_0 - \frac{1}{2}q_p\delta_{ij}\bar{\mathbf{B}}^2/\mu_0. \quad (8)$$

Note in particular the definition of the signs of the terms involving the functions  $q_s(\bar{\mathbf{B}})$  and  $q_p(\bar{\mathbf{B}})$ . This becomes clear when writing down the mean Maxwell stress resulting from both mean and fluctuating fields, *i.e.*,

$$-\bar{B}_i\bar{B}_j/\mu_0 + \frac{1}{2}\delta_{ij}\bar{\mathbf{B}}^2/\mu_0 + \Delta\bar{\Pi}_{ij}^f = -(1-q_s)\bar{B}_i\bar{B}_j/\mu_0 + \frac{1}{2}(1-q_p)\delta_{ij}\bar{\mathbf{B}}^2/\mu_0 + \dots \quad (9)$$

Thus, the signs are defined such that for positive  $q_s$  and  $q_p$  the effects of magnetic stress and magnetic pressure are reduced and the signs of the net effects may even change. Equations (8) and (9) have been derived using the spectral  $\tau$  relaxation approach (Kleeorin, Rogachevskii, and Ruzmaikin, 1990; Kleeorin, Mond, and Rogachevskii, 1996; Rogachevskii and Kleeorin, 2007) and the renormalization procedure (Kleeorin and Rogachevskii, 1994).

A broad range of different DNSs in stratified turbulence (Brandenburg *et al.*, 2011, 2012) or turbulent convection (Käpylä *et al.*, 2011) have now confirmed that  $q_p$  is positive for  $Re_M > 1$ , but  $q_s$  is small and perhaps even negative. A positive value of  $q_s$  (but with large error bars) was originally reported for unstratified turbulence (Brandenburg, Kleeorin, and Rogachevskii, 2010). Later, stratified simulations with isothermal stable stratification (Brandenburg *et al.*, 2012) and convectively unstable stratification (Käpylä *et al.*, 2011) have shown that it is small and negative. Nevertheless,  $q_p(\bar{\mathbf{B}})$  is consistently larger than unity provided  $Re_M > 1$  while  $\bar{B}/B_{eq}$  is below a certain critical value that is around 0.5. This is shown in Figure 9, where we plot the effective magnetic pressure,

$$\mathcal{P}_{eff}(\beta) = \frac{1}{2}[1 - q_p(\beta)]\beta^2 \quad versus \quad \beta \equiv |\bar{\mathbf{B}}|/B_{eq} \quad (10)$$

for different values of  $Re_M$  using  $Pr_M = 0.5$  and  $k_f/k_1 = 15$ . Note that the minimum of  $\mathcal{P}_{eff}(\beta)$  is deeper for the case with  $Re_M = 11$  and then becomes shallower.

Note that  $\beta_{crit}$  is well below unity. This implies that it is probably not possible to produce flux concentrations stronger than half the equipartition field strength. As such, making sunspots with this mechanism alone may be unlikely, and other effects such as that of Kitchatinov and Mazur (2000) may be needed. Such a mechanism would possibly work preferentially in the uppermost layers, provided that enough flux has already been accumulated. This may then be achieved with NEMPI, which also works in somewhat lower layers.

To compare the resulting functions  $\mathcal{P}_{eff}(\beta)$  in a systematic fashion for different parameters, we use the fit formula (Kemel *et al.*, 2012)

$$q_p(\beta) = \frac{q_{p0}}{1 + \beta^2/\beta_p^2} = \frac{\beta_*^2}{\beta_p^2 + \beta^2}, \quad \text{where } \beta_*^2 = q_{p0}\beta_p^2. \quad (11)$$

To describe NEMPI accurately in a mean-field model, the fit should be good at low values of  $\beta$ . In Figure 9 we overplot fits where the parameters  $q_{p0}$  and  $\beta_p$  have been determined such that the minimum is well reproduced. However, note that then the fit becomes poor at larger values of  $\beta$ , provided  $Re_M \gg 1$ .

The resulting dependencies  $\beta_p(Re_M)$ ,  $\beta_*(Re_M)$ , and  $q_{p0}(Re_M)$  are shown in Figure 10 and compared with the results of Brandenburg *et al.* (2012) for  $k_f/k_1 = 5$ . We see that  $\beta_*(Re_M)$  varies relatively little between 0.1 and 0.2 and is typically around 0.15. For small values of  $Re_M$ ,  $\beta_p(Re_M)$  drops from 1 to 0.1 and then stays approximately constant, while  $q_{p0}(Re_M)$

**Figure 9** Normalized effective magnetic pressure,  $\mathcal{P}_{\text{eff}}(\beta)$ , for low (upper panel) and higher (lower panel) values of  $R_{\text{M}}$ . The solid lines represent the fits to the data shown as dotted lines.

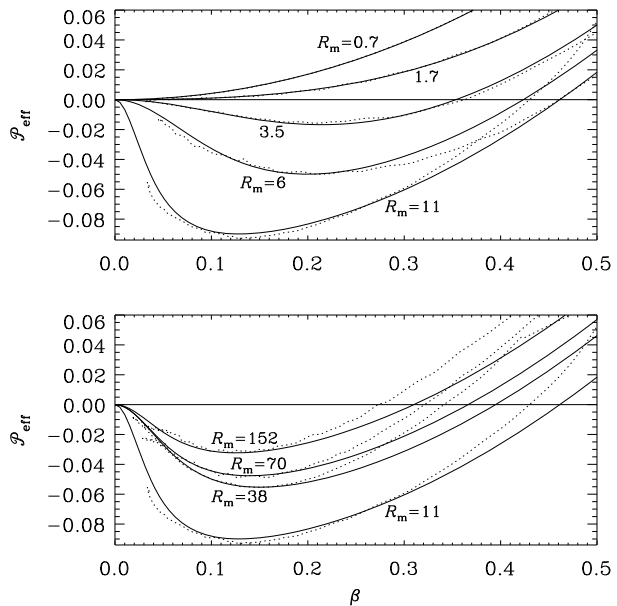
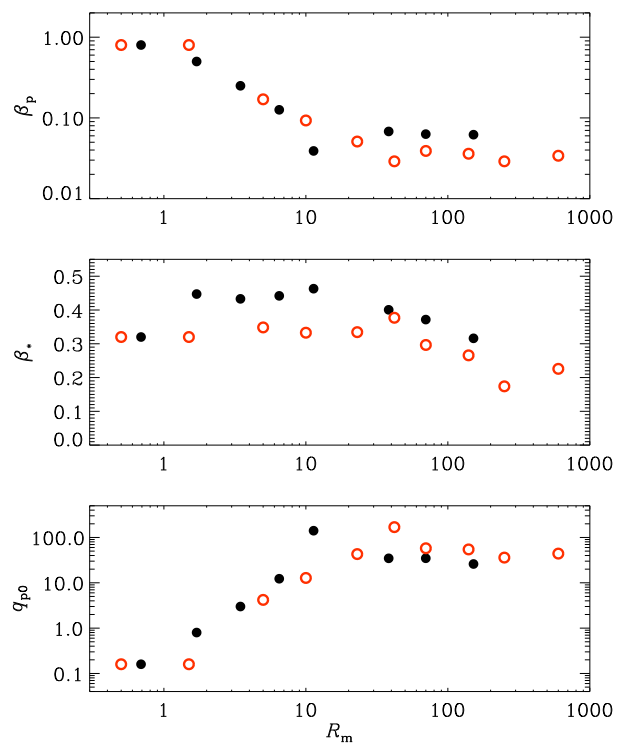


**Figure 10**  $R_{\text{M}}$  dependence of  $\beta_p$ ,  $\beta_*$ , and  $q_{p0}$  for  $P_{\text{rM}} = 0.5$  and  $k_f/k_1 = 15$  (filled symbols) compared with those for  $k_f/k_1 = 5$  (open red symbols) of Brandenburg *et al.* (2012).



rises proportional to  $\text{Re}_M^2$  for  $\text{Re}_M \leq 10$  and then levels off at a value around 40. The values of  $\beta_p$  and  $\beta_*$  are slightly bigger for larger scale separation, while the values of  $q_{p0}$  are more similar.

The significance of a positive  $q_s$  value comes from mean-field simulations with  $q_s > 0$  indicating the formation of three-dimensional (non-axisymmetric) flux concentrations (Brandenburg, Kleeorin, and Rogachevskii, 2010). This result was later identified to be a direct consequence of having  $q_s > 0$  (Kemel et al., 2012). Before making any further conclusions, it is important to assess the effect of other terms that have been neglected. Two of them are related to the vertical stratification, *i.e.* additional terms in Equation (8) that are proportional to  $g_i g_j$  and  $g_i \overline{B}_j + g_j \overline{B}_i$  with  $\mathbf{g}$  being gravity. The coefficient of the former term seems to be small (Käpylä et al., 2011), and the second only has an effect when there is a vertical or inclined imposed magnetic field. However, there could be other terms such as  $\overline{J}_i \overline{J}_j$  when the scale separation is not large enough. Furthermore, in astrophysically relevant situations, the flow will possess helicity, so there can be pseudo-scalar coefficients in front of pseudo-tensors such as  $\overline{J}_i \overline{B}_j$  and  $\overline{J}_j \overline{B}_i$ . Again, none of these effects is well explored yet.

## 5. Conclusions

In this paper we have performed detailed investigations of NEMPI detected recently by BKKMR. Most notably, we have extended the values of the scale separation ratio,  $k_f/k_1$ , from 15 to 30. In this case, the spontaneous formation of magnetic structures becomes particularly evident and can be clearly noticed even without any averaging. Whether or not the particular structures seen in DNS really have a correspondence to phenomena in the Sun cannot be answered at the moment, because our model is still quite unrealistic in many respects. For example, in the Sun,  $k_f$  and  $u_{\text{rms}}$  change with depth, which is not currently taken into account in DNS. Also, of course, the stratification is not isothermal, but convectively unstable. However, DNSs in turbulent convection by Käpylä et al. (2011) have shown that  $\mathcal{P}_{\text{eff}}(\beta)$  still has a negative minimum in that case, and it may even be deeper and wider than in the isothermal case.

Regarding the production of sunspots, it is likely that NEMPI will shut off before the magnetic energy density has reached values comparable with the internal energy of the gas, as is the case in sunspots. Thus, some other mechanism is still needed to push the field of flux concentrations into that regime. One likely candidate is the mechanism of Kitchatinov and Mazur (2000), where the suppression of convective heat flux by the magnetic field is crucial. This impression is further justified by recent calculations of Stein et al. (2011), where pores are seen to form spontaneously in a simulation where horizontal magnetic fields are injected at the bottom of the domain.

Pores are small sunspots, with scales of a few granules, so something else is needed to make these structures bigger and to amplify this mechanism further. Again, the answer could be related to larger scale separation, which would allow NEMPI to operate and to concentrate the magnetic field on scales encompassing many turbulent granules. Thus, even though NEMPI may not suffice to amplify fields to sunspot strengths, it would still be needed to produce active regions out of which sunspots grow by mechanisms such as convective flux suppression, as seen in models of Kitchatinov and Mazur (2000) and simulations of Stein et al. (2011). Thus, it is important to undertake detailed investigations of instabilities in strongly stratified layers with finite heat flux and finite magnetic field.

**Acknowledgements** We thank the anonymous referee for making detailed suggestions. We acknowledge the NORDITA dynamo programs of 2009 and 2011 for providing a stimulating scientific atmosphere. Computing resources were provided by the Swedish National Allocations Committee at the Center for Parallel Computers at the Royal Institute of Technology in Stockholm and the High Performance Computing Center North in Umeå. This work was supported in part by the European Research Council under the AstroDyn Research Project No. 227952.

## References

- Brandenburg, A.: 2005, *Astrophys. J.* **625**, 539.
- Brandenburg, A., Procaccia, I., Segel, D.: 1995, *Phys. Plasmas* **2**, 1148.
- Brandenburg, A., Kleeorin, N., Rogachevskii, I.: 2010, *Astron. Nachr.* **331**, 5.
- Brandenburg, A., Jennings, R.L., Nordlund, Å., Rieutord, M., Stein, R.F., Tuominen, I.: 1996, *J. Fluid Mech.* **306**, 325.
- Brandenburg, A., Kemel, K., Kleeorin, N., Mitra, D., Rogachevskii, I.: 2011, *Astrophys. J.* **740**, L50 (BKKMR).
- Brandenburg, A., Kemel, K., Kleeorin, N., Rogachevskii, I.: 2012, *Astrophys. J.* doi:[10.1088/0004-637X/748/1/1](https://doi.org/10.1088/0004-637X/748/1/1). arXiv:1005.5700.
- Cally, P.S., Dikpati, M., Gilman, P.A.: 2003, *Astrophys. J.* **582**, 1190.
- Cheung, M.C.M., Rempel, M., Title, A.M., Schüssler, M.: 2010, *Astrophys. J.* **720**, 233.
- Cline, K.S., Brummell, N.H., Cattaneo, F.: 2003, *Astrophys. J.* **599**, 1449.
- Golub, L., Rosner, R., Vaiana, G.S., Weiss, N.O.: 1981, *Astrophys. J.* **243**, 309.
- Guerrero, G., Käpylä, P.J.: 2011, *Astron. Astrophys.* **533**, A40.
- Käpylä, P.J., Brandenburg, A., Kleeorin, N., Mantere, M.J., Rogachevskii, I.: 2011, *Mon. Not. Roy. Astron. Soc.* in press. arXiv:1105.5785.
- Kemel, K., Brandenburg, A., Kleeorin, N., Rogachevskii, I.: 2012, *Astron. Nachr.* **333**, 95.
- Kitchatinov, L.L., Mazur, M.V.: 2000, *Solar Phys.* **191**, 325.
- Kitchatinov, L.L., Olemskoy, S.V.: 2006, *Astron. Lett.* **32**, 320.
- Kitiashvili, I.N., Kosovichev, A.G., Wray, A.A., Mansour, N.N.: 2010, *Astrophys. J.* **719**, 307.
- Kleeorin, N., Rogachevskii, I.: 1994, *Phys. Rev. E* **50**, 2716.
- Kleeorin, N.I., Rogachevskii, I.V., Ruzmaikin, A.A.: 1989, *Sov. Astron. Lett.* **15**, 274.
- Kleeorin, N.I., Rogachevskii, I.V., Ruzmaikin, A.A.: 1990, *Sov. Phys. JETP* **70**, 878.
- Kleeorin, N., Mond, M., Rogachevskii, I.: 1996, *Astron. Astrophys.* **307**, 293.
- Newcomb, W.A.: 1961, *Phys. Fluids* **4**, 391.
- Nordlund, Å., Brandenburg, A., Jennings, R.L., Rieutord, M., Ruokolainen, J., Stein, R.F., Tuominen, I.: 1992, *Astrophys. J.* **392**, 647.
- Ossendrijver, M.: 2003, *Astron. Astrophys. Rev.* **11**, 287.
- Parker, E.N.: 1966, *Astrophys. J.* **145**, 811.
- Parker, E.N.: 1979, *Cosmical Magnetic Fields*, Oxford University Press, New York.
- Parker, E.N.: 1982, *Astrophys. J.* **256**, 302.
- Parker, E.N.: 1984, *Astrophys. J.* **283**, 343.
- Priest, E.R.: 1982, *Solar Magnetohydrodynamics*, Reidel, Dordrecht.
- Rempel, M.: 2011a, *Astrophys. J.* **729**, 5.
- Rempel, M.: 2011b, *Astrophys. J.* **740**, 15.
- Rempel, M., Schüssler, M., Knölker, M.: 2009, *Astrophys. J.* **691**, 640.
- Rempel, M., Schüssler, M., Cameron, R.H., Knölker, M.: 2009, *Science* **325**, 171.
- Rogachevskii, I., Kleeorin, N.: 2007, *Phys. Rev. E* **76**, 056307.
- Rüdiger, G.: 1989, *Differential Rotation and Stellar Convection: Sun and Solar-Type Stars*, Gordon & Breach, New York.
- Stein, R.F., Lagerfjärd, A., Nordlund, Å., Georgobiani, D.: 2011, *Solar Phys.* **268**, 271.
- Sur, S., Brandenburg, A., Subramanian, K.: 2008, *Mon. Not. Roy. Astron. Soc.* **385**, L15.
- Tao, L., Weiss, N.O., Brownjohn, D.P., Proctor, M.R.E.: 1998, *Astrophys. J.* **496**, L39.
- Tserkovnikov, Y.A.: 1960, *Sov. Phys. Dokl.* **5**, 87.